

Inline holographic microscopy through fiber imaging bundles

MICHAEL R HUGHES^{1*}

¹Applied Optics Group, School of Physical Sciences, University of Kent, Canterbury. CT2 7NH. United Kingdom

*Corresponding author: m.r.hughes@kent.ac.uk

Compiled June 17, 2020

Fiber imaging bundles are widely used as thin, passive image conduits for miniaturised and endoscopic microscopy, particularly for confocal fluorescence imaging. Holography microscopy through fiber bundles is more challenging; phase conjugation approaches are complex and require extensive calibration. This letter describes how simple inline holographic microscopy can be performed through an imaging bundle using a partially coherent illumination source from a multimode fiber. The sample is imaged in transmission, with the intensity hologram sampled by the bundle and transmitted to a remote camera. The hologram can then be numerically refocused for volumetric imaging, achieving a resolution of approximately 6 μm over a depth range of 1 mm. The scheme does not require any complex prior calibration and hence is insensitive to bending.

<http://dx.doi.org/10.1364/ao.XX.XXXXXX>

1. INTRODUCTION

Holographic microscopy is a simple yet powerful technique in which a sparsely occupied 3D volume can be reconstructed through the acquisition of a single hologram. The hologram captures phase information, providing a contrast mechanism beyond simple absorption, as well as a means of numerical refocusing. Encoding of the phase within the intensity pattern recorded by the camera requires some form of interferometry. In the 'inline' approach to holography, a collimated or diverging beam is scattered by objects within the imaging volume and interferes with the unscattered portion of the beam, directly forming a hologram at the camera. Following the subtraction of a background image, acquired with no sample in the volume, the resulting contrast hologram can then be numerically propagated to reconstruct the intensity of objects at any or all depths within the volume. This common-path approach results in a simple and compact optical arrangement, requiring only a laser source, pinhole and camera; no other optics are required. How-

ever, quantitative recovery of phase is complicated by the twin image artifact, and requires the use of iterative algorithms with prior information such as an estimate of the spatial support of each object [1] or the acquisition of multiple images [2], or else more complicated optical setups such as sideband holography [3].

While inline holography was traditionally performed using long coherence length lasers, a partially coherent source (such as an LED behind a pinhole) is sufficient [4] provided that the object-to-camera distance is kept small (typically up to a few millimeters). The small distance ensures that the scattered light hits the camera within the coherence area of the unscattered light. This simple approach has led to the development of very low cost lensless holographic microscopes, with a range of promising applications including in point-of-care diagnostics [1] and water sample analysis [5]. These devices all require the CCD chip to be placed very close to the sample, and so the minimum size of the microscope is governed by the requirement to include a camera and associated electronics. Despite the portability of these holographic microscopes, they tend to operate on the principle of bringing the sample to the microscope and then mounting it or flowing it through the field-of-view, much as in conventional microscopy.

This letter demonstrates that inline holographic microscopy can be performed using a fiber imaging bundle. Rather than capturing the inline hologram directly with a camera, the hologram is instead relayed to a remote camera. Bundles act as simple image conduits and have been widely used in endoscopic imaging applications for many years. While traditional fiberscope endoscopes have been made obsolete for most applications by the development of compact 'chip-on-tip' cameras, bundles are finding new applications in endoscopic fluorescence microscopy [6]. However, a difficulty with using fiber bundles within coherent imaging systems is that even the bundles with the smallest cores (down to around 2 μm) are typically not single-mode at visible wavelengths [7]. When spatially coherent light is employed, each core therefore generates a small speckle pattern which is highly sensitive to bending or other changes in the configuration of the fiber bundle. For example, it was noted that reflectance mode confocal microscopy through fiber bundles was inferior to spinning disk confocal using a white light source [8]. Optical coherence tomography through fiber bundles is also problematic, both due to modal dispersion (although some fiber bundles are single-mode in the

near infra-red) and cross-talk between cores which tends to degrade interference patterns [7].

More significantly, the phase relationship across a field of light is not maintained by a bundle due to variations in optical path length between each of the fibers, resulting both from varying propagation constants and varying physical lengths. The optical path lengths also change as the fiber bundle is bent or otherwise disturbed. For a given configuration it is possible to measure the relative phase shift between each of the cores and correct for this using a spatial light modulator, allowing remote focusing of a spot at the distal end of the fiber, or recovery of phase at the proximal end [9]. However, this is a complex procedure, requiring recalibration for any disturbance of the fiber bundle, and has yet to find practical applications. A simple form of light field imaging can be implemented by analyzing the azimuthal dependency of power within each core [10], but this does not allow full recovery of phase. Non-quantitative phase contrast imaging for thick tissue using oblique back illumination has also been demonstrated, but does not permit numerical refocusing [11].

In the holographic approach reported in this letter, the imaging procedure is fundamentally different; unlike phase conjugation approaches it does not require complex calibration and is insensitive to bending. The intensity hologram is formed at the distal end of the fiber, requiring only the intensity of the hologram to be transmitted by the bundle. Variations in optical path length between cores, therefore, do not affect the hologram or subsequent image recovery. Further, by use of a source with a short coherence length (an LED) variations in intensity due to the multimodal behavior of the fiber cores are minimized.

A schematic of the optical set-up is shown in Fig. 1. A 450 nm central wavelength, 15 nm bandwidth LED (Thorlabs M450LP1) was coupled into a 50 μm core, 0.22 NA multimode fiber which delivered light to the sample. The tip of the illumination fiber was approximately 15 mm from the tip of the fiber bundle (Fujikura FIGH-30-650S), and the sample was usually placed within 2 mm of the tip of the bundle. The bundle had an active imaging diameter of 600 μm , and contained approximately 30,000 cores arranged in a quasi-hexagonal pattern. The intensity of the inline hologram formed on the fiber bundle was transmitted in pixelated form and imaged onto a monochrome CMOS camera (Thorlabs DCC1545M) via a 20X objective and a 100 mm focal length tube lens. The magnification between the bundle and the camera was 11.8. With a camera pixel size of 5.2 μm , each pixel was projected to a size of approximately 0.44 μm at the bundle, and so the typical 3 μm inter-core spacing of the bundle was sampled by approximately 6 camera pixels. The image of the active area of the bundle was approximately 7.1 mm in diameter at the camera sensor plane. As the camera sensor was 6.66x5.32 mm this meant that the image of the circular bundle was slightly cropped.

Two approaches for removal of the fiber core pattern were investigated. Firstly, a simple Gaussian spatial filter was applied, with a standard deviation chosen to be the minimum at which individual cores can no longer be resolved by eye in the hologram. The second approach, described in detail previously [12], was to interpolate pixel values between the cores. This procedure requires an initial calibration using a background image. A Hough transform is used to identify the center of each of the fiber cores in the calibration image. In practice it was found necessary to first up-sample the image by a factor of 3, giving approximately 12 pixels per core diameter and 18 pixels per core spacing. A Delaunay triangulation is then formed over the core

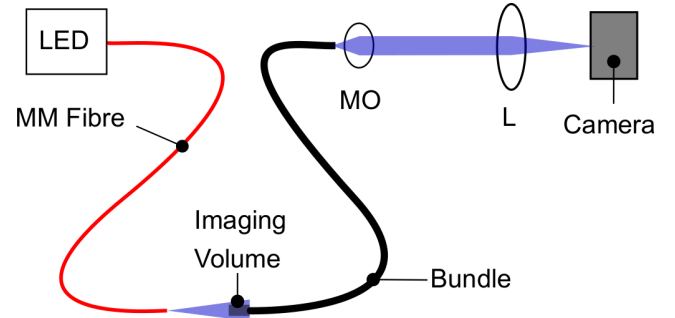


Fig. 1. Setup used to assess feasibility of inline holography via fiber bundle. MO: Microscope objective lens (20X); L: tube lens, achromatic doublet ($f = 100$ mm); Camera: CMOS camera; MM fiber: multimode fiber for illumination; LED: 450 nm fiber-coupled LED.

locations. A reconstruction grid is chosen (in this case corresponding to the pixels in the raw image), the enclosing triangle for each pixel in the reconstruction grid is identified, and the location of the pixel is recorded in barycentric co-ordinates. This concludes the calibration stage.

To process all subsequent holograms, the average intensity is extracted from each core in the image using the pre-calculated core position. This average is taken over the image pixels which lie inside the radius of each core, as determined by the Hough transform. This is then normalised with respect to the intensity value for this core in the calibration image. This step is designed to remove variations in core transmission as well as effects due to any small errors in locating the center of each core. The value of each pixel in the reconstruction grid, I_p , is then obtained by triangular linear interpolation using

$$I_p = I_1 b_1 + I_2 b_2 + I_3 b_3 \quad (1)$$

where I_n is the average intensity from the core lying at the n th vertex of the enclosing triangle, and b_n is the n th pre-computed barycentric co-ordinate of that pixel in relation to the enclosing triangle.

A contrast hologram is obtained by subtracting the reconstructed hologram from a reconstructed background image, taken with no sample in the field-of-view. This reduces spurious artifacts due to edges and variations in the intensity of the illumination source across the field-of-view. Numerical refocusing to a specific depth plane is then performed via the angular spectrum method [13]. Operationally, this is accomplished by taking a Fourier transform of the contrast hologram. This is then multiplied by the complex propagator, and the result is inverse Fourier transformed to obtain the refocused complex field. The absolute value is then taken to obtain the intensity image. Phase images can also be obtained in this way, although without further processing this is not quantitatively correct due to the presence of the twin image.

The propagator in the spatial frequency domain, $P(u, v)$ is defined as [13]

$$P(u, v) = \exp \left[\frac{2\pi i z}{\lambda} \sqrt{1 - (\lambda u)^2 - (\lambda v)^2} \right] \quad (2)$$

where λ is the central wavelength, u, v are spatial frequency coordinates, and z is the refocus distance. Numerical refocusing of a hologram $H(x, y)$ to obtain an image $I(x, y)$ at distance z is

then achieved via

$$I(x,y) = \mathcal{F}^{-1}[\mathcal{F}\{H(x,y)\}P(u,v)] \quad (3)$$

The required refocusing depth for each image was determined automatically using a Brenner gradient-based edge detection metric to identify the best focus. This metric was found to be convex over a good range of refocus depths, allowing the use of a fast bounded search (between 100 μm and 2000 μm) using the golden section method with parabolic interpolation.

Fig. 2 shows examples of holograms and numerically refocused images reconstructed with (a,d) no processing applied, (b,e) a Gaussian filter of 3 pixels (1.32 μm) standard deviation, and (c,f) linear interpolation between cores. The sample was polystyrene microspheres with a nominal diameter of 5 μm which were evaporated onto a 1 mm thick glass slide. Illumination was through the slide (i.e. there was no glass between the microspheres and the fiber bundle.) and the bundle was approximately 0.5 mm from the microspheres. The differences between reconstructions using the three methods are small, and the core pattern is not visible even when no processing is performed, although there is some high frequency noise visible in the zoomed inset. This is in contrast to contact-based imaging through fiber bundles, where the core pattern is prominent unless removed. The two microspheres in the inset are slightly better resolved for the interpolation method over the filtering, although there is scope for further optimisation of the filter to improve this. In what follows the interpolation method is used throughout, but it should be noted that a broadly similar results can be obtained with either no processing or simple spatial filtering.

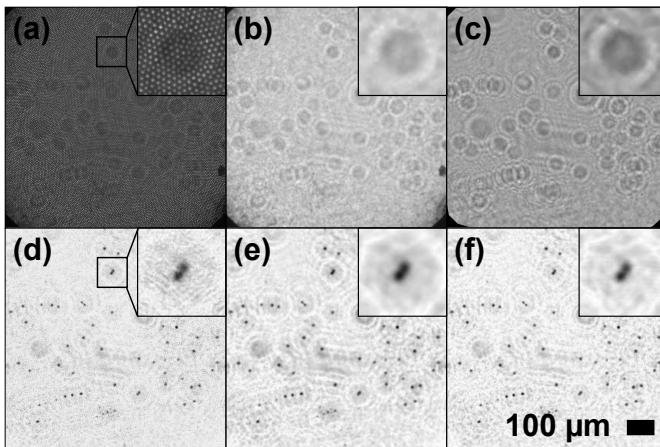


Fig. 2. Inline holograms and numerically refocused reconstructions of 5 μm microspheres on glass slide acquired via fiber bundle. (a), (b) and (c) are holograms; (a) has no pre-processing, (b) has a Gaussian filter of 1.32 μm applied, (c) was linearly interpolated. (d), (e) and (f) are the corresponding numerically refocused images. Insets show a zoom on a 50 \times 50 μm area containing two closely spaced microspheres. Dataset and code available for download in Data 1 (Ref. [14])

A drawback of using fiber bundles for any kind of endoscopic imaging is the finite core or pixel count in the resulting images. The largest flexible bundles typically have around 30,000 cores, resulting in a circular image with a diameter of only around 200 pixels. In inline holography the resolution is usually limited by camera pixel size and the magnification of

the interference fringe pattern onto the camera. For partially coherent sources the requirement to place the camera close to the sample means that, in practice, little better than unit magnification can be achieved. An analysis then determines the resolution to be similar or slightly better than the pixel pitch [1]. In the fiber bundle holographic microscope, the fiber bundle core spacing becomes the limiting factor in resolution, since the other end of the bundle can be imaged onto a camera with arbitrary magnification. A resolution comparable to the fiber core spacing is therefore expected.

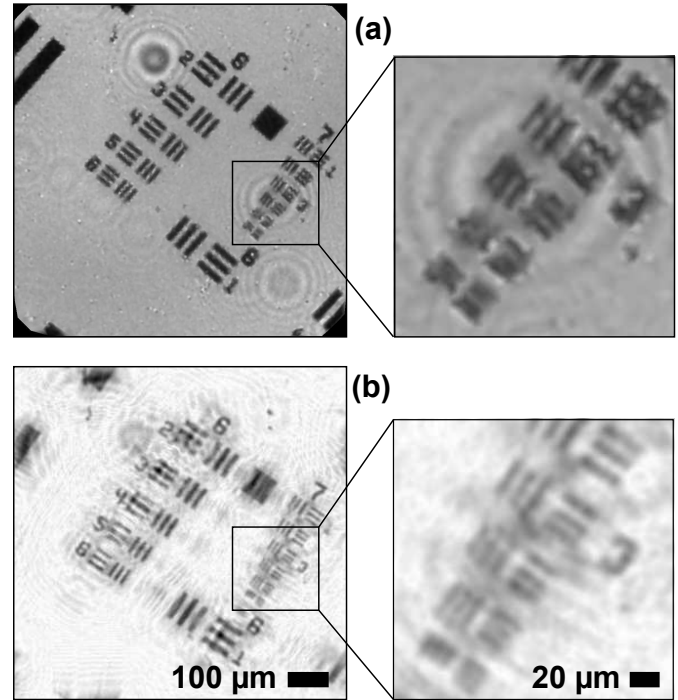


Fig. 3. Images of USAF resolution target captured through fiber bundle. (a) USAF resolution target placed in direct contact with the bundle. (b) USAF resolution target at a distance of 0.75 mm from the bundle face and numerically refocused. Dataset and code available for download in Data 2 (Ref. [15])

To assess the resolution, fig. 3 shows groups 6 and 7 of a USAF resolution target. In (a) the target was placed in direct contact with the fiber bundle (i.e. no numerical refocusing was required), while in (b) it was placed at a distance of 0.75 mm from the tip of the bundle and the image was numerically refocused. Based on the typical core-core spacing of 3 μm , Nyquist sampling limits suggests a resolution of approximately 6 μm for the direct contact image, corresponding to group 7 element 3 (specified as 6.20 μm). This element is clearly resolved, while element 4 (5.52 μm) is at the borderline of visibility. For the numerically-refocused inline holography image (b), element 4 (5.52 μm) is clearly resolved and element 5 (4.92 μm) is at the limit of visibility. The resolution obtained through inline holography and numerical refocusing is therefore similar or slightly better than conventional contact imaging.

As with all inline holography systems based on partially-coherent illumination, there is a finite allowable working distance between the sample and the detector (in this case the bundle). Fig. 4 shows the measured size of 5 μm microspheres as a function of their distance from the bundle face. Microspheres were evaporated onto a glass stage, as for fig. 2, which

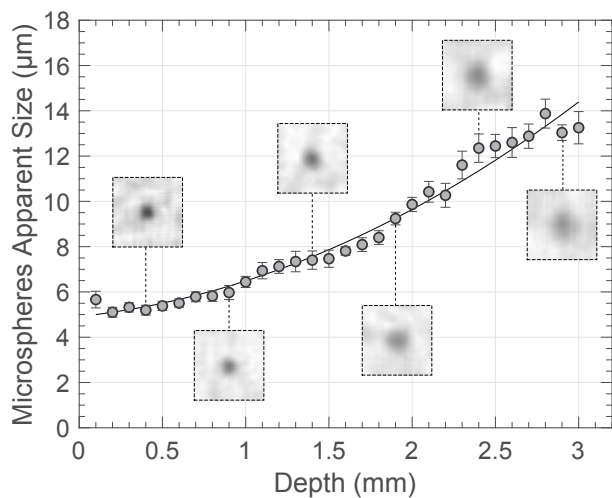


Fig. 4. Effect on resolution of distance of sample from bundle face, determined by apparent size of $5\ \mu\text{m}$ diameter microsphere. Values are mean full-width half-maximum across 10 spheres, error bars are standard error, trend line is 2nd order polynomial (least squares fit). Insets show example images of one of the spheres at six selected depths ($27\times 27\ \mu\text{m}$ ROI). Dataset and code available for download in Data 3 (Ref. [16])

was then moved away from the bundle using a translation stage. The best focus for each image was found using the same Brenner-based algorithm as described above, but constrained to be within $200\ \mu\text{m}$ of the expected depth. To obtain the diameter of the spheres at each depth, the centre of each microspheres was taken to be the point of highest signal and the value of each pixel within a $70\times 70\ \mu\text{m}$ ROI around the centre was plotted as a function of its distance from the centre. The microsphere size was then taken to be the full-width half-maximum (FWHM) of this plot.

This measurement was repeated across 10 individual microspheres to obtain the mean FWHM values shown in the plot. The trend-line is a least-squares fit of a 2nd order polynomial ($R^2 = 0.98$). Example images of one of the microspheres at selected distances are shown for illustration. It can be seen that resolution of better than $7\ \mu\text{m}$ is obtained within a distance of approximately $1\ \text{mm}$ from the tip of the bundle, increasing to $10\ \mu\text{m}$ at approximately $2\ \text{mm}$ from the tip. This is in agreement with the result from the USAF target of a resolution of approximately $5.5\ \mu\text{m}$ at a distance $0.75\ \text{mm}$, shown in fig. 3. This degradation of resolution with distance from the bundle is an expected consequence of using partially coherent illumination. The resolution also appears to degrade slightly very close to the bundle face, likely due to the impact of the fiber cores.

To demonstrate the potential of the device for water imaging, the fiber was inserted into a tray of water collected from a small freshwater pond on the University of Kent campus. Fig. 5 shows an example frame from Visualisation 1, a video of 130 frames acquired at 10 fps. A moving object was tracked using a simple motion identification procedure which involved subtraction of successive frames, Gaussian filtering, and identification of the resulting ‘peak’ difference. A $55\times 55\ \mu\text{m}$ region of interest was extracted around the moving object and the depth of the object identified using the Brenner-based algorithm described above (constrained between 0.1 and $0.5\ \text{mm}$). The whole frame

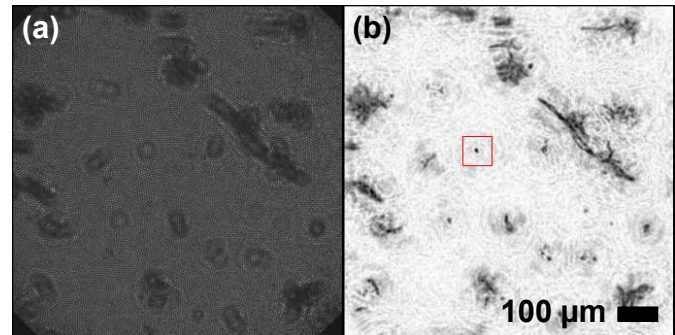


Fig. 5. Numerically refocused hologram from sample of pond water. The focal position was chosen for visualisation of the object identified within the square. Video sequence showing auto-focusing on the object can be seen in Visualisation 1. Dataset and code available for download in Data 4 (Ref. [17])

was then numerically refocused to this depth and a $40\times 40\ \mu\text{m}$ box drawn around the tracked object for visualization.

These results have demonstrated that it is feasible to use a fiber imaging bundle to collect inline holograms and that the hologram quality is sufficient to allow microscopy intensity images to be reconstructed with resolution comparable to twice the fiber bundle core spacing. A limitation of the probe design is that it requires fibers protruding from each end, limiting the geometries into which it could be deployed. It may be possible to route the two fibers co-axially with a reflector used to redirect the illumination light towards the fiber bundle. In this letter, only intensity image retrieval has been demonstrated, and further work will be required to determine whether twin artifact removal for quantitative phase recovery is practical for fiber bundle holography.

Disclosures The author declares no conflicts of interest.

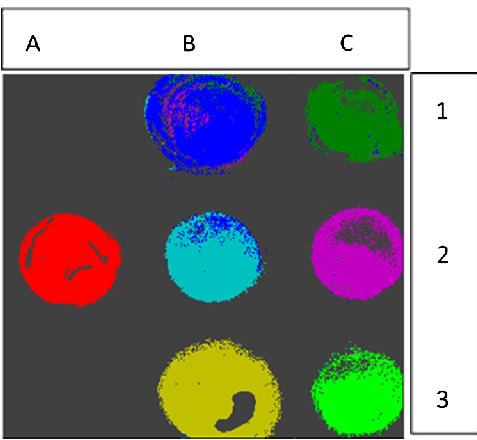
REFERENCES

- O. Mudanyali, D. Tseng, C. Oh, S. O. Isikman, I. Sencan, W. Bishara, C. Oztoprak, S. Seo, B. Khademhosseini, and A. Ozcan, *Lab on a Chip* **10**, 1417 (2010).
- A. Greenbaum, N. Akbari, A. Feizi, W. Luo, and A. Ozcan, *PLoS one* **8** (2013).
- C. Ramirez, A. Lizana, C. Lemmi, and J. Campos, *Opt. Lett.* **40**, 4142 (2015).
- L. Repetto, E. Piano, and C. Pontiggia, *Opt. Lett.* **29**, 1132 (2004).
- Z. Göröcs, M. Tamamitsu, V. Bianco, P. Wolf, S. Roy, K. Shindo, K. Yanny, Y. Wu, H. C. Koydemir, Y. Rivenson *et al.*, *Light. Sci. & Appl.* **7**, 1 (2018).
- J. M. Jabbour, M. A. Saldua, J. N. Bixler, and K. C. Maitland, *Annals Biomed. Eng.* **40**, 378 (2012).
- L. M. Wurster, L. Ginner, A. Kumar, M. Salas, A. Wartak, and R. A. Leitgeb, *J. Biomed. Opt.* **23**, 066001 (2018).
- R. Juškatis, T. Wilson, and T. Watson, *Scanning* **19**, 15 (1997).
- E. R. Andresen, S. Sivankutty, V. Tsvirkun, G. Bouwmans, and H. Rigneault, *J. Biomed. Opt.* **21**, 121506 (2016).
- A. Orth, M. Ploschner, E. Wilson, I. Maksymov, and B. Gibson, *Sci. Adv.* **5**, eaav1555 (2019).
- T. N. Ford, K. K. Chu, and J. Mertz, *Nat. Methods* **9**, 1195 (2012).
- M. R. Hughes, P. Giataganas, and G.-Z. Yang, *J. Biomed. Opt.* **19**, 030501 (2014).
- T. Latychevskaia and H.-W. Fink, *Appl. Opt.* **54**, 2424 (2015).
- M. R. Hughes, *Inline holographic microscopy through a fiber imaging bundle*, *Fig 2* (2020). <https://doi.org/10.6084/m9.figshare.12280169.v1>.

15. M. R. Hughes, *Inline holographic microscopy through a fiber imaging bundle, Fig 3* (2020).
[Http://dx.doi.org/10.6084/m9.figshare.12280169](http://dx.doi.org/10.6084/m9.figshare.12280169).
16. M. R. Hughes, *Inline holographic microscopy through a fiber imaging bundle, Fig 4* (2020).
[Http://dx.doi.org/10.6084/m9.figshare.12280169](http://dx.doi.org/10.6084/m9.figshare.12280169).
17. M. R. Hughes, *Inline holographic microscopy through a fiber imaging bundle, Fig 5* (2020).
[Http://dx.doi.org/10.6084/m9.figshare.12280169](http://dx.doi.org/10.6084/m9.figshare.12280169).

FULL REFERENCES

1. O. Mudanyali, D. Tseng, C. Oh, S. O. Isikman, I. Sencan, W. Bishara, C. Oztoprak, S. Seo, B. Khademhosseini, and A. Ozcan, "Compact, light-weight and cost-effective microscope based on lensless incoherent holography for telemedicine applications," *Lab on a Chip* **10**, 1417–1428 (2010).
2. A. Greenbaum, N. Akbari, A. Feizi, W. Luo, and A. Ozcan, "Field-portable pixel super-resolution colour microscope," *PloS one* **8** (2013).
3. C. Ramirez, A. Lizana, C. Lemmi, and J. Campos, "Inline digital holographic movie based on a double-sideband filter," *Opt. Lett.* **40**, 4142–4145 (2015).
4. L. Repetto, E. Piano, and C. Pontiggia, "Lensless digital holographic microscope with light-emitting diode illumination," *Opt. Lett.* **29**, 1132–1134 (2004).
5. Z. Göröcs, M. Tamamitsu, V. Bianco, P. Wolf, S. Roy, K. Shindo, K. Yanny, Y. Wu, H. C. Koydemir, Y. Rivenson *et al.*, "A deep learning-enabled portable imaging flow cytometer for cost-effective, high-throughput, and label-free analysis of natural water samples," *Light. Sci. & Appl.* **7**, 1–12 (2018).
6. J. M. Jabbour, M. A. Saldua, J. N. Bixler, and K. C. Maitland, "Confocal endomicroscopy: instrumentation and medical applications," *Annals Biomed. Eng.* **40**, 378–397 (2012).
7. L. M. Wurster, L. Ginner, A. Kumar, M. Salas, A. Wartak, and R. A. Leitgeb, "Endoscopic optical coherence tomography with a flexible fiber bundle," *J. Biomed. Opt.* **23**, 066001 (2018).
8. R. Juškattis, T. Wilson, and T. Watson, "Real-time white light reflection confocal microscopy using a fibre-optic bundle," *Scanning* **19**, 15–19 (1997).
9. E. R. Andresen, S. Sivankutty, V. Tsvirkun, G. Bouwmans, and H. Rigneault, "Ultrathin endoscopes based on multicore fibers and adaptive optics: a status review and perspectives," *J. Biomed. Opt.* **21**, 121506 (2016).
10. A. Orth, M. Ploschner, E. Wilson, I. Maksymov, and B. Gibson, "Optical fiber bundles: Ultra-slim light field imaging probes," *Sci. Adv.* **5**, eaav1555 (2019).
11. T. N. Ford, K. K. Chu, and J. Mertz, "Phase-gradient microscopy in thick tissue with oblique back-illumination," *Nat. Methods* **9**, 1195 (2012).
12. M. R. Hughes, P. Giataganas, and G.-Z. Yang, "Color reflectance fiber bundle endomicroscopy without back-reflections," *J. Biomed. Opt.* **19**, 030501 (2014).
13. T. Latychevskaia and H.-W. Fink, "Practical algorithms for simulation and reconstruction of digital in-line holograms," *Appl. Opt.* **54**, 2424–2434 (2015).
14. M. R. Hughes, *Inline holographic microscopy through a fiber imaging bundle, Fig 2* (2020). <https://doi.org/10.6084/m9.figshare.12280169.v1>.
15. M. R. Hughes, *Inline holographic microscopy through a fiber imaging bundle, Fig 3* (2020). <http://dx.doi.org/10.6084/m9.figshare.12280169>.
16. M. R. Hughes, *Inline holographic microscopy through a fiber imaging bundle, Fig 4* (2020). <http://dx.doi.org/10.6084/m9.figshare.12280169>.
17. M. R. Hughes, *Inline holographic microscopy through a fiber imaging bundle, Fig 5* (2020). <http://dx.doi.org/10.6084/m9.figshare.12280169>.



This figure "spheres.png" is available in "png" format from:

<http://arxiv.org/ps/2006.09296v1>